IEEE Photonics Journal
An IEEE Photonics Society Publication

Open Access

Impact of Out-of-Band Noise on OSNR Measurement Using Brillouin Optical Spectrum Analyzer and Its Mitigation Method

Volume 10, Number 5, September 2018

Yibo Zhong
Sheng Cui
Changjian Ke
Zhen Guo
Chen Xing
Haoyu Wang
Keyuan Yang
Deming Liu

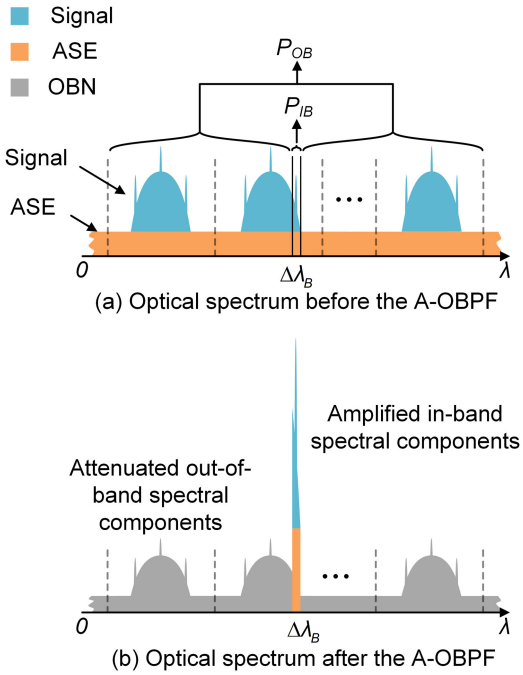

(a) Optical spectrum before the A-OBPF

(b) Optical spectrum after the A-OBPF

DOI: 10.1109/JPHOT.2018.2872954
1943-0655

Impact of Out-of-Band Noise on OSNR Measurement Using Brillouin Optical Spectrum Analyzer and Its Mitigation Method

Yibo Zhong,[1,2] Sheng Cui,[1,2] Changjian Ke,[1,2] Zhen Guo,[1,2] Chen Xing,[1,2] Haoyu Wang,[1,2] Keyuan Yang,[1,2] and Deming Liu[1,2]

[1]School of Optical and Electronic Information, Huazhong University of Science and Technology, Wuhan 430074, China
[2]National Engineering Laboratory for Next Generation Internet Access System, Huazhong University of Science and Technology, Wuhan 430074, China

DOI:10.1109/JPHOT.2018.2872954

Manuscript received August 24, 2018; revised September 26, 2018; accepted September 26, 2018. Date of publication October 1, 2018; date of current version October 12, 2018.This work is supported by the National Natural Science Foundation of China under Grant 61475053. Corresponding authors: Sheng Cui and Changjian Ke (e-mail: cuisheng@hust.edu.cn; cjke@mail.hust.edu.cn).

Abstract: Brillouin optical spectrum analyzer (BOSA) based on stimulated Brillouin scattering (SBS) can provide ultra-high resolution, which in theory can greatly improve the optical signal-to-noise ratio (OSNR) measurement accuracy, especially for systems with close channel spacing and cascaded filtering effect (CFE). BOSA utilizes narrow bandwidth SBS as an active optical band-pass filter (A-OBPF); thus, the unwanted out-of-band spectral components are actually not completely suppressed and may account for an unneglectable proportion of the spectral power filtered out, especially for broadband multi-channel signals. Such out-of-band noise (OBN) will degrade the OSNR measurement accuracy. In this paper, the OBN impact on both interpolation and reference optical spectrum (ROS) based OSNR measurement methods are investigated theoretically and experimentally. An effective mitigation method of OBN impact is then proposed and verified by experiments.

Index Terms: Brillouin optical spectrum analyzer (BOSA), out-of-band noise, optical signal-to-noise ratio (OSNR), optical performance monitoring (OPM), optical spectrum (OS), cascaded filtering effect (CFE).

1. Introduction

Optical performance monitoring (OPM) is indispensable for robust and intelligent optical networks [1]. Optical signal-to-noise ratio (OSNR) is the most important OPM parameter as the other distortions like chromatic dispersion (CD) and polarization mode dispersion (PMD) can be compensated in digital coherent optical receivers [2]. The traditional standardized OSNR monitoring method uses optical spectrum analyzers (OSA) to measure the amplified spontaneous emission (ASE) noise optically by interpolating the noise level from the spectral gaps between signals. However, this method is not adequate for ultra-dense wavelength division multiplexing (ultra-DWDM) or super-channel systems because the common resolution of the diffraction grating based optical spectrum analyzer (OSA) is about 0.06 nm under which the spectral gap may be blurred or invisible, so the

noise level can't be determined accurately. Furthermore, in systems employing add/drop filters or wavelength selective switches (WSS) the ASE noise at the spectral gap may be highly suppressed due to cascaded filtering effect (CFE), making the interpolation method ineffective [3].

To solve these problems, various OSNR measurement methods have been proposed by now [4]–[8]. These methods can be classified into two main types. The first type is based on linear or nonlinear optical schemes, such as polarization-nulling techniques [4], an optical delay interferometer (ODI) [5], a non-linear loop mirror [6], a fiber parametric device [7], [8] or an optical detector designed for two-photo absorption [9]. While the second type uses coherent optical receivers embedded with advanced digital signal processor (DSP) [10]–[12]. Each of these methods has its pros and cons. For the first type of methods, they are bit rate transparent and are relatively cost-effective for wide deployment in the network. But some of them are not suitable for polarization-multiplexed (PM) signals, while the others are not robust to the transmission distortions, like CD, PMD, CFE and nonlinear effect (NLE). For the second type of methods, they are robust to CD, PMD and NLE because these distortions can be compensated or excluded by advanced DSP algorithms. But using such methods OSNR can only be measured within the coherent receiver. To deploy such OSNR monitors widely across the network including the intermediate nodes will be too costly and impractical.

With the maturity of the ultra-high resolution stimulated Brillouin scattering (SBS) based OSA (BOSA) [13]–[18], the aforementioned problems facing the traditional OSA based method can also be solved by replacing the conventional diffraction grating based OSAs with BOSA. BOSA utilizes narrow bandwidth SBS as an active optical band-pass filter (A-OBPF). The spectral components within the A-OBPF bandwidth are amplified by SBS, while the out-of-band components are not and thus equivalently suppressed. As SBS has a gain bandwidth of about 10 MHz, BOSA can provide a spectral resolution of about 0.1 pm [13]. Within BOSA even very narrow spectral gap can be clearly presented [14]–[16], so theoretically the noise level can be determined more accurately. When CFE is present, the reference optical spectrum (ROS) based OSNR measurement methods can be used [3], [19]–[23]. They rely on a detailed spectral comparison between the noise-free ROS which is measured near the transmitter and the one measured at the desired OSNR monitoring point. The ROS based methods are suitable for PM signals and are robust to various distortions including CFE, CD, PMD and fiber nonlinear effects [19]–[21]. But to achieve the best accuracy, OBPFs with GHz or sub-GHz bandwidth are required [19], [20]. Such OBPFs are expensive and not commercially available at present. It is proposed that via coherent receptions finer electrical filters can be used to replace the ultra-narrow bandwidth OBPF by filtering the signal in electrical domain [20]. In BOSA this requirement can be easily satisfied directly in the optical domain. Thus in theory BOSA is very suitable for both interpolation and ROS based methods.

But different from passive OBPF, the optical rejection ratio of the A-OBPF is determined by the SBS gain on the in-band spectral components. The unwanted out-of-band spectral components are actually not completely suppressed and may account for an unneglectable proportion of the spectral power filtered out, especially for broadband DWDM or superchannel signals with a total power much larger than the spectral components extracted with the ultra-narrow A-OBPF. Such out-of-band noise (OBN) in BOSA will degrade the accuracy of OSNR measurement. In this paper the impact of OBN on the accuracy of the interpolation and ROS based OSNR measurement methods are analyzed theoretically and experimentally. An OBN impact mitigation method is also proposed. Experiments are then carried out to validate the effectiveness of this method.

2. Impact of OBN on OSNR Measurement

The definition of OSNR is given by the following equation

$$OSNR = 10\log_{10}\left(\frac{P_S}{P_{ASE}}\right). \tag{1}$$

Here P_S represents the signal power and P_{ASE} represents the ASE noise power within the reference bandwidth $\Delta\lambda_{ref}$ equal to 0.1 nm. For systems without CFE the ASE noise levels within

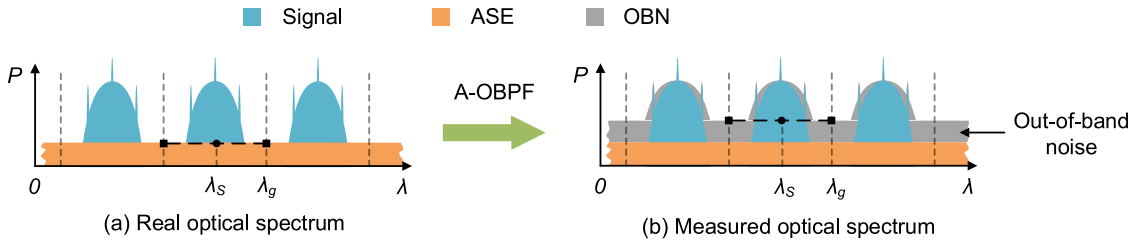

Fig. 1. The schematic diagram of the working principle of the interpolation based OSNR monitoring method (a). The OBN impact on the measured spectrum (b).

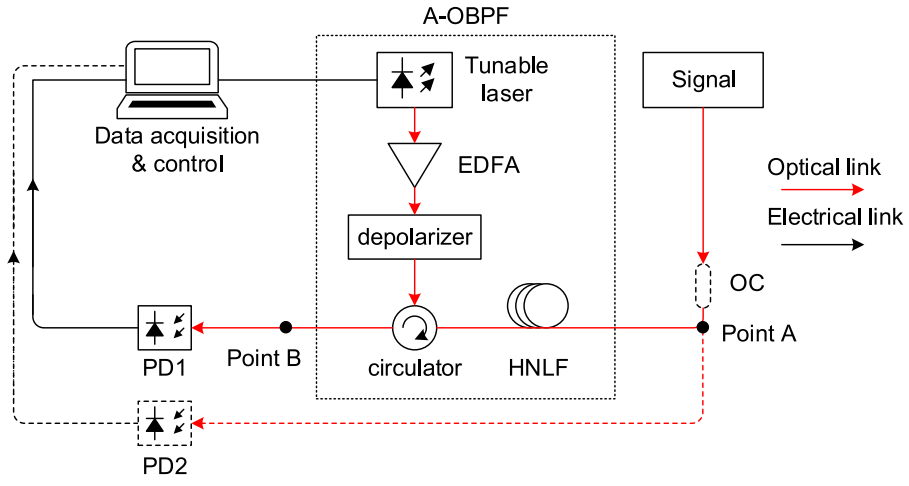

Fig. 2. The schematic diagrams of the typical BOSA setup (solid line) and improved one with OBN mitigation function (solid and dashed line). PD: photo detector, EDFA: erbium doped fiber amplifier, HNLF: highly nonlinear fiber, OC: optical coupler.

the signal bandwidth and at the spectral gap are nearly the same as schematically shown in Fig. 1(a), thus the interpolation method can be used. For systems with CFE, ROS based method should be used and it will be investigated later. First for systems without CFE, assuming OBN can be neglected for the time being, P_S and P_{ASE} can be obtained by Eqs. (2) and (3).

$$P_S = \int_{\lambda_S - \frac{\Delta\lambda_S}{2}}^{\lambda_S + \frac{\Delta\lambda_S}{2}} P_M(\lambda)\, d\lambda - \frac{\Delta\lambda_S}{\Delta\lambda_{ref}} P_{ASE}, \tag{2}$$

$$P_{ASE} = \int_{\lambda_g - \frac{\Delta\lambda_{ref}}{2}}^{\lambda_g + \frac{\Delta\lambda_{ref}}{2}} P_M(\lambda)\, d\lambda. \tag{3}$$

Here $P_M(\lambda)$ is the optical spectrum obtained by BOSA. $\Delta\lambda_S$ represents the signal bandwidth, λ_S and λ_g represent the central wavelengths of the signal and spectral gap. The second item on the right of Eq. (2) represents the ASE noise power within the signal bandwidth. Fig. 1(a) shows the real signal and ASE noise spectra when CFE is not present, while the measured spectra obtained with BOSA is schematically shown in Fig. 1(b). It is obvious that they are different. The orange part represents the real ASE noise while the gray part represents the extra OBN caused by the unwanted spectral components outside the A-OBPF's pass band. OBN increases the noise level observed by BOSA as shown in Fig. 1(b). In the following section the formation mechanism of OBN is first investigated.

With regard to optical spectrum measurement, the schematic diagram of the typical setup of BOSA is shown in Fig. 2 (the part plotted with solid line). It consists of a tunable laser source (TLS),

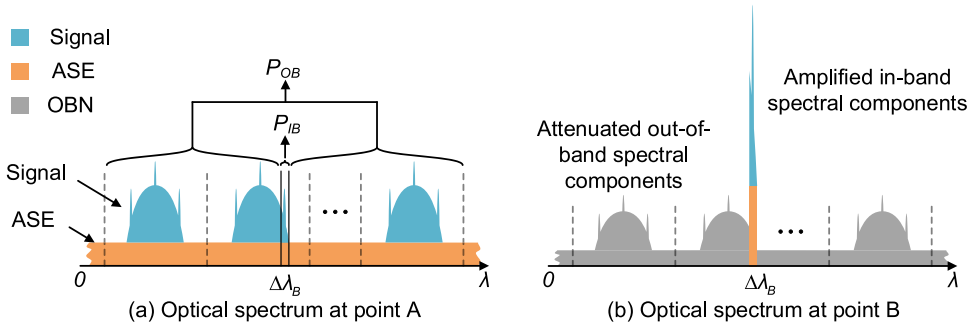

Fig. 3. The optical spectra before the A-OBPF, i.e., at point A (a) and after the A-OBPF, i.e., at point B (b).

erbium doped fiber amplifier (EDFA), depolarizer, highly nonlinear fiber (HNLF), optical circulator, optical detector and conventional data acquisition and control system [14], [15]. The TLS is used as the pump. It generates SBS gain within a narrow bandwidth of about 10 MHz in the highly nonlinear fiber (HNLF) that amplifies the backward propagating signal. The spectra before and after the equivalent A-OBPF are shown in Fig. 3. The amplified signal is selected by the optical circulator and input into the optical detector for power measurement. The whole spectrum is measured by tuning the pump wavelength to shift the center wavelength (λ) of the SBS-based A-OBPF and recording the corresponding output signal power $P_M(\lambda)$ with data acquisition system. As shown in Fig. 3(b), $P_M(\lambda)$ consists of the spectral powers of the components within (colored) and out-of (gray) the A-OBPF bandwidth $\Delta\lambda_B$. The out-of-band one $P_{OB}(\lambda)$ is equal to the total input power P_T over the whole input spectrum subtracted by the in-band one $P_{IB}(\lambda)$ within $\Delta\lambda_B$. Thanks to SBS $P_{IB}(\lambda)$ is amplified by a gain of G, while the out-of-band one $P_{OB}(\lambda)$ is attenuated by a factor of *Att* due to the optical link loss from point A to point B as shown in Fig. 2. The rejection ratio *R* of the A-OBPF is given by $R = G^*Att$. $P_M(\lambda)$ can thus be written as follows

$$P_M(\lambda) = G P_{IB}(\lambda) + \frac{1}{Att} P_{OB}(\lambda), \tag{4}$$

$$P_{IB}(\lambda) = P_S(\lambda) + P_{ASE}(\lambda), \tag{5}$$

$$P_{OB}(\lambda) = P_T - P_{IB}(\lambda) \approx P_T. \tag{6}$$

Here $P_{S,ASE}(\lambda)$ represent the signal and ASE noise powers within the BOSA resolution bandwidth $\Delta\lambda_B$. For broadband DWDM or superchannel signals $P_T >> P_{IB}(\lambda)$ as the latter is measured within only about 10 MHz. Thus $P_{OB}(\lambda)$ is approximately equal to P_T. So $P_{OB}(\lambda) >> P_{IB}(\lambda)$. This means OBN represented by the second item on the right of Eq. (4) may account for an unneglectable proportion of $P_M(\lambda)$ even when *R* is large. As a result, in the measured spectrum the noise level is higher than the real ASE noise level as shown in Fig. 1(b). Thus OSNR measurement based on Eqs. (1–3) will be affected by OBN in BOSA.

Considering OBN, for systems without CFE the real signal and ASE noise powers are given by

$$P_S = \int_{\lambda_S - \frac{\Delta\lambda_S}{2}}^{\lambda_S + \frac{\Delta\lambda_S}{2}} P_M(\lambda)\, d\lambda - \frac{\Delta\lambda_S}{\Delta\lambda_{ref}} P_{ASE} - \frac{1}{Att} \int_{\lambda_S - \frac{\Delta\lambda_S}{2}}^{\lambda_S + \frac{\Delta\lambda_S}{2}} P_{OB}(\lambda)\, d\lambda, \tag{7}$$

$$P_{ASE} = \int_{\lambda_g - \frac{\Delta\lambda_{ref}}{2}}^{\lambda_g + \frac{\Delta\lambda_{ref}}{2}} P_M(\lambda)\, d\lambda - \frac{1}{Att} \int_{\lambda_g - \frac{\Delta\lambda_{ref}}{2}}^{\lambda_g + \frac{\Delta\lambda_{ref}}{2}} P_{OB}(\lambda)\, d\lambda. \tag{8}$$

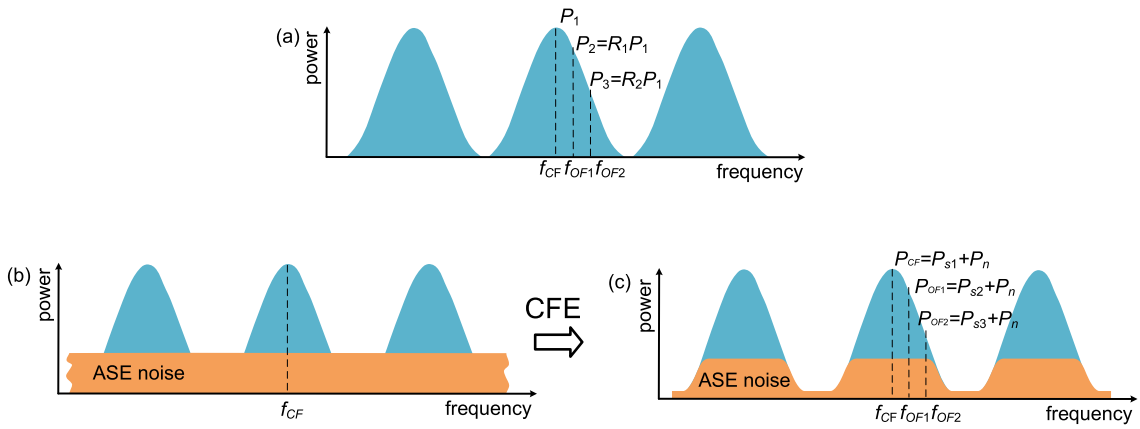

Fig. 4. The Schematic diagram of the working principles of the ROS based OSNR monitoring method. The noise-free ROS measured at the transmitter (a). The signal optical spectrum with accumulated ASE noise when CFE is not present (b) and present (c).

The last item on the right of Eqs. (7) and (8) represents the OBN power within the signal and noise reference bandwidth $\Delta\lambda_s$ and $\Delta\lambda_{ref}$. Using Eqs. (4–6), Eqs. (7–8) can be rewritten as follows.

$$\begin{aligned}
P_S &= \int_{\lambda_S-\frac{\Delta\lambda_S}{2}}^{\lambda_S+\frac{\Delta\lambda_S}{2}} P_M(\lambda)\,d\lambda - \frac{\Delta\lambda_S}{\Delta\lambda_{ref}} P_{ASE} - \frac{1}{Att}\int_{\lambda_S-\frac{\Delta\lambda_S}{2}}^{\lambda_S+\frac{\Delta\lambda_S}{2}} P_{OB}(\lambda)\,d\lambda \\
&= \int_{\lambda_S-\frac{\Delta\lambda_S}{2}}^{\lambda_S+\frac{\Delta\lambda_S}{2}} P_M(\lambda)\,d\lambda - \frac{\Delta\lambda_S}{\Delta\lambda_{ref}}\left[\int_{\lambda_g-\frac{\Delta\lambda_{ref}}{2}}^{\lambda_g+\frac{\Delta\lambda_{ref}}{2}} P_M(\lambda)\,d\lambda - \frac{1}{Att}\int_{\lambda_g-\frac{\Delta\lambda_{ref}}{2}}^{\lambda_g+\frac{\Delta\lambda_{ref}}{2}} P_{OB}(\lambda)\,d\lambda\right] - \frac{1}{Att}\int_{\lambda_S-\frac{\Delta\lambda_S}{2}}^{\lambda_S+\frac{\Delta\lambda_S}{2}} P_{OB}(\lambda)\,d\lambda \\
&\approx \int_{\lambda_S-\frac{\Delta\lambda_S}{2}}^{\lambda_S+\frac{\Delta\lambda_S}{2}} P_M(\lambda)\,d\lambda - \frac{\Delta\lambda_S}{\Delta\lambda_{ref}}\int_{\lambda_g-\frac{\Delta\lambda_{ref}}{2}}^{\lambda_g+\frac{\Delta\lambda_{ref}}{2}} P_M(\lambda)\,d\lambda + \frac{1}{Att}\int_{\lambda_S-\frac{\Delta\lambda_S}{2}}^{\lambda_S+\frac{\Delta\lambda_S}{2}} P_T\,d\lambda - \frac{1}{Att}\int_{\lambda_S-\frac{\Delta\lambda_S}{2}}^{\lambda_S+\frac{\Delta\lambda_S}{2}} P_T\,d\lambda \\
&= \int_{\lambda_S-\frac{\Delta\lambda_S}{2}}^{\lambda_S+\frac{\Delta\lambda_S}{2}} P_M(\lambda)\,d\lambda - \frac{\Delta\lambda_S}{\Delta\lambda_{ref}}\int_{\lambda_g-\frac{\Delta\lambda_{ref}}{2}}^{\lambda_g+\frac{\Delta\lambda_{ref}}{2}} P_M(\lambda)\,d\lambda, \qquad (9)
\end{aligned}$$

$$\begin{aligned}
P_{ASE} &= \int_{\lambda_g-\frac{\Delta\lambda_{ref}}{2}}^{\lambda_g+\frac{\Delta\lambda_{ref}}{2}} P_M(\lambda)\,d\lambda - \frac{1}{Att}\int_{\lambda_g-\frac{\Delta\lambda_{ref}}{2}}^{\lambda_g+\frac{\Delta\lambda_{ref}}{2}} P_{OB}(\lambda)\,d\lambda \\
&\approx \int_{\lambda_g-\frac{\Delta\lambda_{ref}}{2}}^{\lambda_g+\frac{\Delta\lambda_{ref}}{2}} P_M(\lambda)\,d\lambda - \frac{1}{Att}\int_{\lambda_g-\frac{\Delta\lambda_{ref}}{2}}^{\lambda_g+\frac{\Delta\lambda_{ref}}{2}} P_T\,d\lambda. \qquad (10)
\end{aligned}$$

Eq. (9) is the same as Eq. (2) which shows that P_S can be directly obtained from measured spectrum $P_M(\lambda)$ as if OBN was not present. Eq. (10) shows that the OBN item must be eliminated, otherwise OSNR will be underestimated. Recalling that the measured spectrum $P_M(\lambda)$ has a resolution bandwidth of $\Delta\lambda_B$, the OBN item in Eq. (10) can be approximately given by

$$P_{OBN}^{I} \approx \frac{1}{Att}\int_{\lambda_g-\frac{\Delta\lambda_{ref}}{2}}^{\lambda_g+\frac{\Delta\lambda_{ref}}{2}} P_T\,d\lambda \approx \frac{P_T\Delta\lambda_{ref}}{\Delta\lambda_B Att}. \qquad (11)$$

For systems with CFE, the ASE noise level at the spectral gap may be highly suppressed and is not equal to the one within the signal bandwidth as shown in Fig. 4. In this case the ROS based method can be used [19]–[23]. Fig. 4(a) shows the noise-free ROS measured near the transmitter. The ROS shape and the power ratios $R_1 = P_2/P_1$ and $R_2 = P_3/P_1$ are determined by the type of optical signal. Here $P_{1,2,3}$ are the signal spectral powers measured at frequencies of f_{CF}, f_{OF1} and

f_{OF2} using a tunable band-pass filter (BPF) with bandwidth of $\Delta\lambda_R$. Here f_{CF} represents the signal center frequency, and $f_{OF1,2}$ represent two offset frequencies from f_{CF}. Numerical and experimental investigations show that a higher accuracy can be obtained when the spectral power is measured within about 500 MHz bandwidth ($\Delta\lambda_R \approx 4$ pm) [20]. This can be easily satisfied in BOSA by integration of $P_M(\lambda)$ over the desired $\Delta\lambda_R$. As shown in Fig. 4(c) the measured spectral powers for signals with ASE noise can be expressed as

$$\begin{aligned} P_{CF} &= P_{s1} + P_n, \\ P_{OF1} &= P_{s2} + P_{n2} = R_1\alpha^N P_{s1} + P_n, \\ P_{OF2} &= P_{s3} + P_{n3} = R_2\beta^N P_{s1} + P_n. \end{aligned} \tag{12}$$

where $P_{s1,s2,s3}$ represent the signal spectral powers (not including the noise) within $\Delta\lambda_R$ at frequencies of f_{CF}, f_{OF1} and f_{OF2}. Assuming the ASE noise spectrum is flat within the signal bandwidth P_n is used to represent the ASE noise spectral powers at f_{CF}, f_{OF1} and f_{OF2}. The weighting factor α^N and β^N are introduced to depict the CFE on the signal OS. Here α and β are the spectral transmission coefficients of the intermediate filtering elements at f_{OF1} and f_{OF2}, respectively. N is the total number of the filtering elements. It is noteworthy that a more accurate model considering CFE on ASE spectrum is proposed in [23]. For concision it is not discussed in this paper. But the method proposed in this paper is also suitable for that OSNR measurement model. By solving Eq. (12), we can obtain N, P_{s1} and P_n and thus calculate the in-band OSNR [20].

Because Eq. (12) have no analytical solution, to analytically investigate the OBN impact on OSNR measurement, it is assumed that $\alpha = \beta = 1$, in other words, the filtering elements have a flat top. In this case, Eq. (12) can be simplified to

$$\begin{aligned} P_{CF} &= P_{s1} + P_n, \\ P_{OF} &= R_1 P_{s1} + P_n. \end{aligned} \tag{13}$$

So OSNR is given by

$$OSNR = \gamma\frac{P_{s1}}{P_n} = \gamma\frac{(P_{OF} - P_{CF})/(R_0 - 1)}{P_{CF} - (P_{OF} - P_{CF})/(R_0 - 1)} = \gamma\frac{(P_{OF} - P_{CF})}{(R_0 - 1)P_{CF} - (P_{OF} - P_{CF})}. \tag{14}$$

where the calibration parameter γ is determined by $\Delta\lambda_R$ and $\Delta\lambda_S$ [20]. In BOSA, $P_{CF,OF}$ can be obtained by integration over the same bandwidth of $\Delta\lambda_R$, thus they contain approximately the same amount of OBN power. For this reason, only the first item in the denominator of Eq. (14) is changed by OBN, leading to underestimated OSNR. Similarly as Eq. (11), the OBN power within $\Delta\lambda_R$ is approximately given by

$$P_{OBN}^{R} \approx \frac{\Delta\lambda_R P_T}{\Delta\lambda_B Att}. \tag{15}$$

In summary to mitigate the OBN impact on the interpolation and ROS based methods $P_{OBN}^{I,R}$ given by Eqs. (11) and (15) must be measured. To solve this problem, the new BOSA setup as shown in Fig. 2 is proposed. A small portion of the input signal is tapped off the main link at the input of the A-OBPF by an optical coupler and input into the extra optical detector to estimate P_T. The other parameter *Att* representing the attenuation from point A to B in Fig. 2 can be readily measured with a power meter. With the two parameters obtained, $P_{OBN}^{I,R}$ can be obtained and used to mitigate the OBN impact on the OSNR measurement.

3. Experimental Results and Discussion

The experimental setup is shown in Fig. 5. The setup of BOSA is the same as that shown in Fig. 1, except that a dual-stage SBS-based A-OBPF is utilized to replace the conventional single-stage one, in order to mitigate the SBS gain saturation [15]. The resolution bandwidth $\Delta\lambda_B$ of the self-made BOSA [15]–[17] used in the experiment is set at 0.1 pm. To measure the attenuation coefficient *Att*

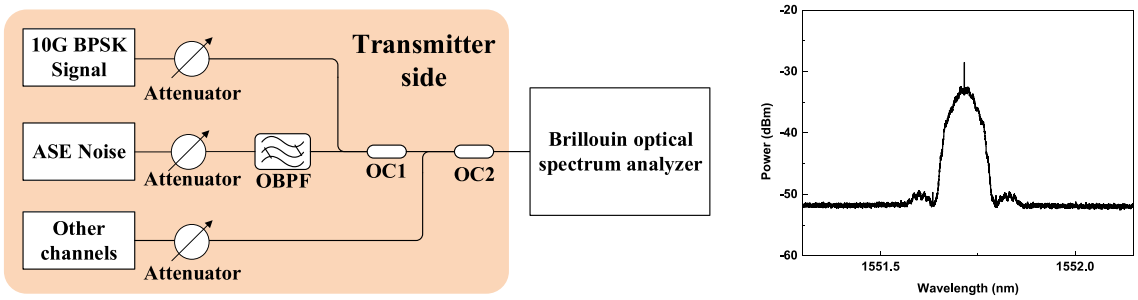

Fig. 5. The experimental setup (a) and the measured optical spectrum of 10 Gbps NRZ-BPSK signal (b).

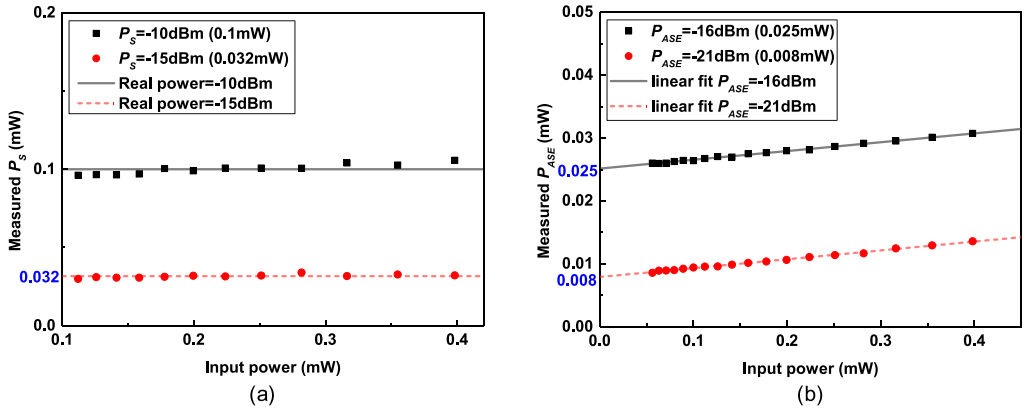

Fig. 6. The measured signal (a) and ASE noise (b) power of channel under test against different total input power.

of the out-of-band components in this dual-stage A-OBPF, a continuous wave optical signal with power of 5 dBm is input into the A-OBPF at point A when the pump is not injected. *Att* can be then obtained by measuring the output power at point B. It is found that *Att* is equal to 48.5 dB for the self-made BOSA. The optical signal under test is 10 Gbps NRZ-BPSK signal which is generated using a DFB diode laser and a Mach-Zehnder modulator. An exemplary ultra-high resolution signal spectrum obtained by the BOSA is shown in Fig. 5(b). As we can see the spectrum has spectral lines (impulses). Ideally BPSK signal spectra shouldn't have such spectral lines because their constellations are symmetric relative to the origin of the complex plane. But due to the non-ideal transmitters, the spectral lines exist in practice [18]. It is noteworthy that such spectral lines are only visible under ultra-high resolution. The ASE noise is generated by an EDFA and loaded onto the optical signal through the first optical coupler (OC1). The other WDM channels with 100 GHz grid are added through the second coupler (OC2). The powers of the signal, ASE noise and the other WDM channels are controlled by the three tunable optical attenuators (TOAs).

First using Eqs. (2) and (3), the signal and ASE noise power $P_{S,ASE}$ for the channel under test are measured against different total input power P_T. The input power of the signal is fixed at -10 and -15 dBm respectively. The ASE noise power within 1 nm is fixed at -16 and -21 dBm, respectively. The experimental results are show in Fig. 6. As we can see the measured value of P_S keeps nearly constant, while that of P_{ASE} increases linearly with P_T due to increasing OBN. Here $\Delta\lambda_B = 0.1$ pm, $\Delta\lambda_{ref} = 0.1$ nm and $Att = 48.5$ dB. According to Eqs. (10) and (11), the slope of the curve should be 0.0141. The slopes of the fitted experimental curves shown in Fig. 6(b) are 0.0140, agreeing very well with the aforementioned analytical result.

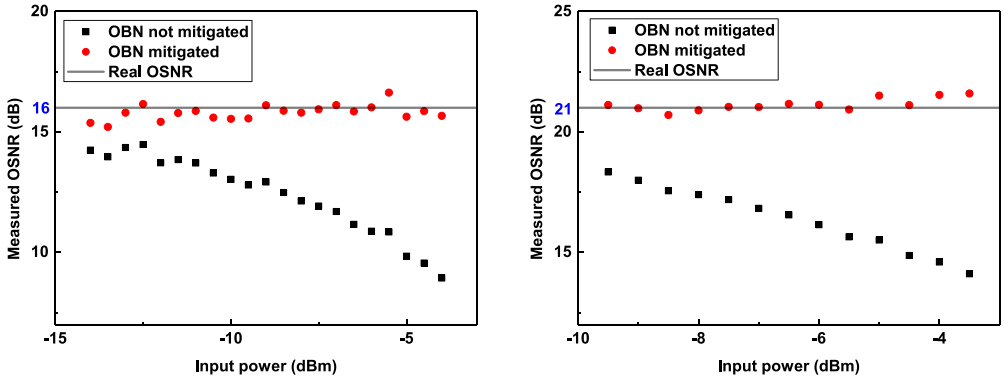

Fig. 7. The measured OSNR against different input power with interpolation based method when OSNR = 16 (a) and OSNR = 21 (b) respectively.

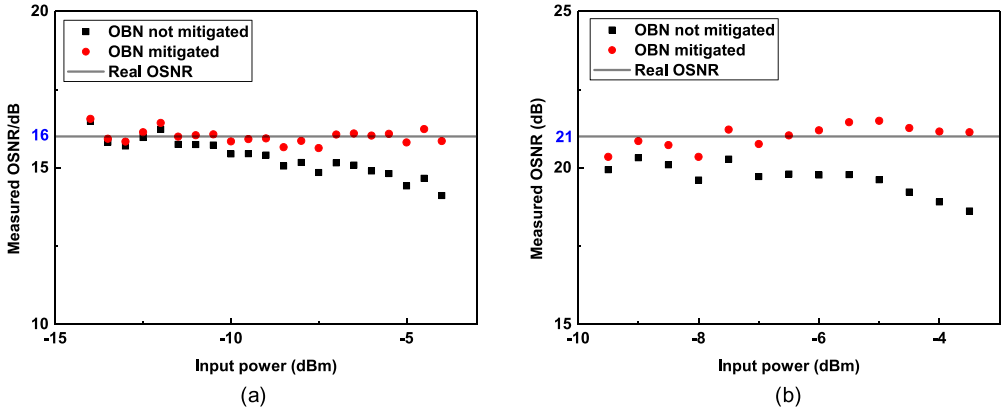

Fig. 8. The measured OSNR against different input power with the ROS based method, when OSNR = 16 (a) and OSNR = 21 (b), respectively.

In the next step, we fixed the signal OSNR at 16 and 21 dB, respectively, and measured it against the total input power P_T. The experimental results obtained with the interpolation and ROS based methods are shown in Fig. 7 and Fig. 8 respectively. As shown in Fig. 7 with the interpolation based method when OBN is not mitigated, the OSNR obtained is underetimated and keeps decreasing with increasing P_T due to OBN. The maximal variation of OSNR measured at a fixed OSNR due to different P_T is about 3 dB and 2 dB for OSNR = 16 and 21 dB, respectively. This input power dependent variation makes the calibration very difficult. After using the proposed method to mitigate OBN impact the measured results represented by the curves formed by the red dots become flatter. As shown in Fig. 7(a) and (b), with the proposed OBN mitigation method the deviation from the real value is greatly reduced and is below 0.8 and 0.5 dB for OSNR = 16 and 21 dB, respectively. Fig. 8 shows that the ROS based method is less affected by OBN. The input power dependent difference is about 1.2 dB and 0.9 dB for OSNR = 16 and 21 dB, respectively, when OBN is not mitigated. With the proposed OBN mitigate method the deviation is reduced to below 0.5 dB and 0.6 dB for OSNR = 16 and 21 dB, respectively.

To further investigate the performance of the proposed method, the OSNR of the channel under test is varied from 10 to 30 dB by increasing the signal power while maintaining the ASE noise power. P_T is also changed by varying the total transmitted power of the other WDM channels. The OSNR measurement results with the original interpolation based method (OBN not mitigated) are

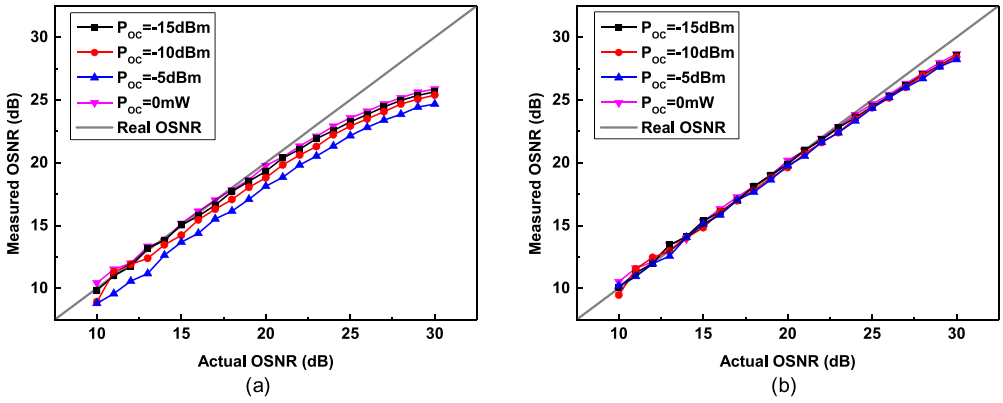

Fig. 9. The measured OSNR with interpolation based method against the actual OSNR. Results obtained with the original interpolation based method (OBN not mitigated) (a). Results obtained with the proposed method (OBN mitigated) (b).

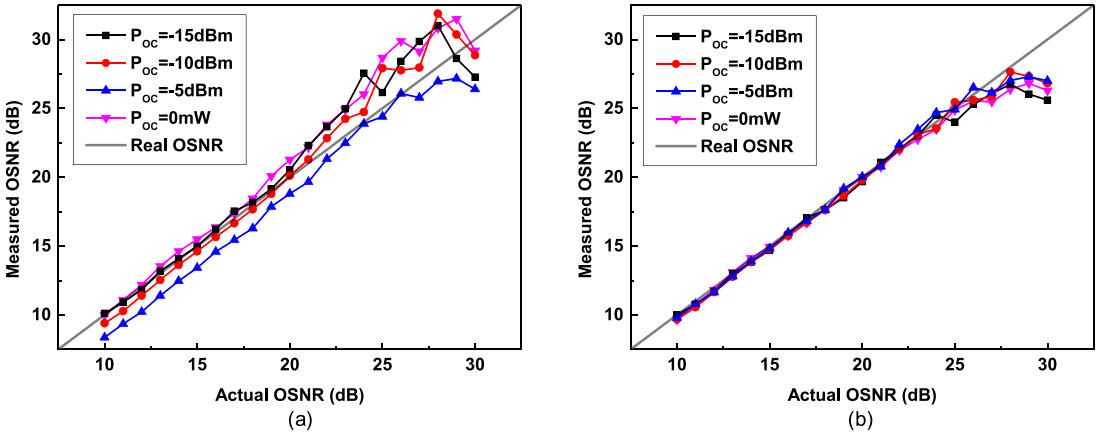

Fig. 10. The measured OSNR with ROS based method against the actual OSNR. Results obtained with the original ROS based method (OBN not mitigated) (a). Results obtained with the proposed method (OBN mitigated) (b).

shown in Fig. 9(a). The curves tend to become flatter at very high OSNR. This is because at high OSNR, the total WDM signal power becomes very high so that the OBN power is much higher than the ASE noise power, thus the measured noise power is approximately equal to the OBN noise power. As the OBN power, as well as the input signal power P_T, increases with OSNR, the measured OSNR becomes nearly constant and is severely underestimated at very high OSNR. Furthermore the maximal difference between the curves measured under different P_T is about 2 dB due to the OBN. This input power dependent variation makes the calibration very difficult. With the proposed method the OBN impact is greatly reduced, and as shown in Fig. 9(b), the curves become more linearly in the high OSNR region and nearly overlapped with each other for different P_T. After calibration the maximal error is below 0.6 dB for OSNR in the interesting range of 10–23 dB.

The results obtained with the ROS based method is shown in Fig. 10. The OBN impact is different from that shown in Fig. 9(a). The curves become more diverged rather than flatter at high OSNR. The difference between the curves is about 2 dB and 5 dB within the low and very high OSNR regions, respectively. With the proposed OBN mitigation method the gap of difference is greatly reduced. The maximal difference is reduced below 1.5 dB at very high OSNR. Below 23 dB the curves nearly overlap with each other. After calibration the maximal error is below 0.5 dB for OSNR in the interesting range of 10–23 dB.

4. Conclusion and Discussion

The formation mechanism of OBN in BOSA and its impact on OSNR measurement are systematically investigated in this paper. The OBN items affect the accuracy of the interpolation and ROS based OSNR measurement methods are deduced. The analytical and experimental results show that due to OBN the OSNR will be underestimated and the measured results will vary with the total input power. To solve this problem a new BOSA setup enabling OBN power estimation and mitigation is proposed. Experimental results show that the accuracy and stability of the two OSNR measurement methods are greatly improved with the proposed OBN impact mitigation method.

References

[1] Z. Dong, F. N. Khan, Q. Sui, K. Zhong, C. Lu, and A. P. T. Lau, "Optical performance monitoring: a review of current and future technologies," *J. Lightw. Technol.*, vol. 34, no. 2, pp. 525–543, Jan. 2016.

[2] S. J. Savory, "Digital coherent optical receivers: algorithms and subsystems," *IEEE J. Sel. Topics Quantum Electron.*, vol. 16, no. 5, pp. 1164–1179, Sep./Oct. 2010.

[3] D. Gariépy, G. He, and G. W. Schinn, "Non-intrusive measurement of in-band OSNR of high bitrate polarization-multiplexed signals," *Opt. Fiber Technol.*, vol. 17, no. 5, pp. 518–522, Oct. 2011.

[4] J. H. Lee, D. K. Jung, C. H. Kim, and Y. C. Chung, "OSNR monitoring technique using polarization-nulling method," *IEEE Photon. Technol. Lett.*, vol. 13, no. 1, pp. 88–90, Jan. 2001.

[5] X. Liu, Y. H. Kao, S. Chandrasekhar, I. Kang, S. Cabot, and L. L. Buhl, "OSNR monitoring method for OOK and DPSK based on optical delay interferometer," *IEEE Photon. Technol. Lett.*, vol. 19, no. 15, pp. 1172–1174, Aug. 2007.

[6] R. Adams, M. Rochette, T. T. Ng, and B. J. Eggleton, "All-optical in-band OSNR monitoring at 40 Gb/s using a nonlinear optical loop mirror," *IEEE Photon. Technol. Lett.*, vol. 18, no. 3, pp. 469–471, Feb. 2006.

[7] T. T. Ng, J. L. Blows, M. Rochette, J. A. Bolger, I. Littler, and B. J. Eggleton, "In-band OSNR and chromatic dispersion monitoring using a fibre optical parametric amplifier," *Opt. Exp.*, vol. 13, no. 14, pp. 5542–5552, Jul. 2005.

[8] S. Cui, S. Sun, L. Li, J. Li, Q. You, and D. Liu, "All-optical in-band optical signal-to-noise monitoring method based on degenerated four-wave mixing," *IET Optoelectron.*, vol. 6, no. 2, pp. 107–109, 2012.

[9] S. Wielandy, M. Fishteyn, and B. Zhu, "Optical performance monitoring using nonlinear detection," *J. Lightw. Technol.*, vol. 22, no. 3, pp. 784–793, Mar. 2004.

[10] M. S. Faruk, Y. Mori, and K. Kikuchi, "In-band estimation of optical signal-to-noise ratio from equalized signals in digital coherent receivers," *IEEE Photon. J.*, vol. 4, no. 1, Feb. 2014, Art. no. 7800109.

[11] D. Zhao, L. Xi, X. Tang, W. Zhang, Y. Qiao, and X. Zhang, "Periodic training sequence aided in-band OSNR monitoring in digital coherent receiver," *IEEE Photon. J.*, vol. 6, no. 4, Aug. 2014, Art. no. 7902009.

[12] L. Dou *et al.*, "An accurate nonlinear noise insensitive OSNR monitor," in *Proc. Opt. Fiber Commun. Conf. (Opt. Soc. Amer.)*, Mar. 2016, Paper W3A.5.

[13] J. M. S. Domingo, J. Pelayo, F. Villuendas, C. D. Heras, and E. Pellejer, "Very high resolution optical spectrometry by stimulated Brillouin scattering," *IEEE Photon. Technol. Lett.*, vol. 17, no. 4, pp. 855–857, Apr. 2005.

[14] Aragon Photonics, "The true High Resolution Optical Spectrum Analyzer." 2018. [Online]. Available: https://aragonphotonics.com/bosa-400-series-optical-spectrum-analyzer

[15] K. Zhang, C. Ke, D. Pan, and D. Liu, "High Resolution and Selectivity SBS-based Filter Utilizing a Dual-stage Scheme," in *Proc. Opt. Fiber Commun. Conf. (Opt. Soc. Amer.)*, Mar. 2016, Paper W3E.5.

[16] C. Xing, C. Ke, K. Zhang, Z. Guo, Y. Zhong, and D. Liu, "Polarization- and wavelength-independent SBS-based filters for high resolution optical spectrum measurement," *Opt. Exp.*, vol. 25, no. 18, pp. 20969–20982, Sep. 2017.

[17] K. Zhang, Y. Zhong, C. Ke, and D. Liu, "High-input dynamic range and selectivity stimulated Brillouin scattering-based microwave photonic filter utilizing a dual-stage scheme," *Opt. Lett.*, vol. 42, no. 17, pp. 3287–3290, Sep. 2017.

[18] H. Lu, S. Cui, C. Ke, and D. Liu, "Automatic reference optical spectrum retrieval method for ultra-high resolution optical spectrum distortion analysis utilizing integrated machine learning techniques," *Opt. Exp.*, vol. 25, no. 26, pp. 32491–32503, Dec. 2017.

[19] S. Oda *et al.*, "In-band OSNR monitor using an optical bandpass filter and optical power measurements for superchannel signals," in *Proc. Eur. Conf. Exhib. Opt. Commun.*, Sep. 2013, pp. 1–3.

[20] Z. Dong *et al.*, "Modulation-format-independent OSNR monitoring insensitive to cascaded filtering effects by low-cost coherent receptions and RF power measurements," *Opt. Exp.*, vol. 23, no. 12, pp. 15971–15982, Jun. 2015.

[21] D. Gariépy, S. Searcy, G. He, and S. Tibuleac, "Non-intrusive OSNR measurement of polarization-multiplexed signals with spectral shaping and subject to fiber non-linearity with minimum channel spacing of 37.5 GHz," *Opt. Exp.*, vol. 24, no. 18, pp. 20156–20166, Sep. 2016.

[22] Z. Huang *et al.*, "A novel in-band OSNR measurement method based on normalized autocorrelation function," *IEEE Photon. J.*, vol. 10, no. 2, Apr. 2018, Art. no. 7903208.

[23] G. Yin, S. Cui, C. Ke, and D. Liu, "Reference optical spectrum based In-Band OSNR monitoring method for EDFA amplified multispan optical fiber transmission system with cascaded filtering effect," *IEEE Photon. J.*, vol. 10, no. 3, Jun. 2018, Art. no. 7201910.